Acta Mech 234, 6297–6314 (2023)
https://doi.org/10.1007/s00707-023-03665-5

ORIGINAL PAPER

Jimmy Aramendiz · Alexander Fidlin

On the vibration control of semi-active friction dampers with piecewise defined contact geometries

Received: 4 February 2023 / Revised: 22 May 2023 / Accepted: 17 July 2023 / Published online: 19 September 2023

Abstract Suppressing unwanted vibrations has been a major challenge for more than a century. Semi-active dampers offer a compromise between the high energy costs of active solutions and their increased flexibility. A nonlinear system that utilizes dry friction and piecewise defined contact geometries is used as the basis for a semi-active damper. Furthermore, a slow frequency-based control that does not solely rely on dissipation is considered and compared to the conventional Skyhook Control. Simulations show that the strategy is an effective approach for vibration reduction.

1 Introduction

The use of efficient dampers reduces vibration amplitudes, resulting in lighter and more efficient machines. These machines produce higher quality products at lower costs. In addition, reduced vibration also leads to longer machine life and therefore less unplanned downtime. There is therefore a financial motive in the research of vibration reduction. Environmental motives stem from the energy efficiency objectives required by politics. There is therefore great interest in reducing unnecessary energy costs of machines. Friction dampers help to achieve this goal and make effective use of dry friction. In particular, the investigations into these devices help to better understand the role of friction in reducing vibrations and represent an effective vibration reduction solution. Compared to their viscous counterparts, friction dampers are less sensitive to changes in temperature and more robust in harsh environments, such as wedge dampers in trains [1] and platform dampers in turbines [2]. Furthermore, they do not require fluid sealing and do not have to deal with leakage [3]. Another advantage of these mechanisms is their amplitude-dependent behavior. These dampers start dissipating energy after a breakaway force is reached [4,5]. This results in dampers that do not continuously dissipate energy, but instead only when necessary. This characteristic is relevant for dampers in the force flow of machines. However, in specific cases, the advantages these dampers provide are not sufficient. Such cases include situations in which extremely low vibration amplitudes are required. For such amplitudes, high friction coefficients are essential to dissipate energy and reduce vibration. However, if a long service life is required, low friction coefficients are the better choice, since they reduce wear in the friction contact. Since low friction coefficients cannot ensure an adequate vibration reduction, a counterbalancing that meets all criteria may not always be viable. Alternatives that reduce vibration in a more effective manner are required, and a semi-active consideration of such dampers offers such an alternative.

J. Aramendiz (✉)· A. Fidlin
Institute of Engineering Mechanics, Karlsruhe Institute of Technology, Kaiserstraße 10, 76131 Karlsruhe, Germany
E-mail: jimmy.aramendiz@kit.edu

A. Fidlin
E-mail: alexander.fidlin@kit.edu

Friction-based dampers have been mainly implemented in a passive manner. A survey of these passive implementations in vibration damping and vibration isolation was presented by Ferri [6]. He categorized the applications of friction dampers into four categories: turbomachinery systems, built-up structures, seismic structures, and railroad applications. However, such dampers have also been considered in their semi-active variants, in which often the normal force of the friction contact is modulated. Lane and Ferri proposed an optimal control and afterward clipped the desired input since for unilateral contacts the normal force is strictly positive [7]. Dupont et al. [8] used a Lyapunov function-based controller to maximize the energy dissipation in the controllable term and derived a corresponding bang–bang control. This controller was very similar to the Skyhook Control proposed by Karnopp [9]; however, it was used for vibration dissipation instead of vibration isolation. Both the clipped optimal control and the Skyhook Control were implemented by Gaul et al. [10] to reduce vibrations in the joints of truss structures. For an impulse perturbation, the clipped linear quadratic controller showed a faster reduction of vibration amplitudes. An alternative approach when controlling friction dampers is to prevent sticking. Such control approaches calculate the necessary normal load for stiction and set the actual normal load slightly under this limit. This strategy was simulated by Lu [11] to reduce seismic vibrations. Experiments with this control strategy also in the context of seismic vibration were performed by Lin et al. [12]. Inaudi [13] proposed an active friction damper with modulated normal force that resulted in a linearly scalable response as with linear viscous damping. To this end, the normal force is chosen proportional to the last local peak. Laffranchi et al. [14] modulated the normal force in the joints of humanoid robots to emulate viscous damping. This literature overview shows that the control strategies in combination with friction dampers are mainly dissipation-oriented. Control strategies that do not solely focus on dissipation and consider vibration absorption and changes in the system's eigenfrequencies via sticking were not noted.

This work considers a semi-active implementation of a friction damper, the semi-active tuned wedge damper. It is characterized by piecewise defined contact surfaces. Its passive form shows an amplitude-dependent behavior that utilizes absorption at low amplitudes and introduces damping at high vibration amplitudes. The vibration reduction capabilities of the passive implementation are expanded by considering its semi-active implementation. Additionally, a slow frequency-based control strategy that does not solely focus on damping is suggested and compared to the conventional Skyhook Control. To study the semi-active tuned wedge damper, first, the base system for the control strategies and the framework for the simulations are presented in Sect. 2. Second, the Skyhook Control is considered in Sect. 3. This is a well-investigated control strategy and is taken as a reference point for the control strategy developed in this work. Third, in Sect. 4 focuses on a slow frequency-based control. The efficiency of the control strategies with respect to the amplitude reduction are compared in Sect. 5, whereas a consideration of the dissipated and consumed energy is made in Sect. 6. The investigations conclude in Sect. 7 with an assessment of the control strategies. For a detailed investigation of the passive tuned wedge damper, the reader is referred to [15].

2 Base system for the control strategies

This section presents the general conditions for the investigations of the semi-active system and is divided into two parts. First, the base system, on which the control strategies are applied, is presented. Additionally, the input parameters as well as their effect on the damper force are detailed. The second part presents the framework of the simulations that are used to investigate the control strategies. This includes the excitation types, the initial conditions, and the constant damper parameters.

The semi-active tuned wedge damper is presented in Fig. 1. The main system is represented by the main mass m_1 and the main spring c_1. It is also excited by the force $F(t)$. From the control point of view, this is a perturbation on the otherwise resting main system. It is the task of the semi-active system to counter this perturbation. To this end, the semi-active wedge damper is attached to the main system. The friction damper is composed of the secondary mass m_2, the secondary spring c_2, the tertiary spring c_3 (with its prestress displacement $\Delta\ell$), and the contact surfaces. The last component is defined by the wedge angle α, the length of the horizontal segment $2\Delta_1$, and the radius of the transition segments r. The positions of the main and secondary mass are, respectively, described by x_1 and x_2.

The controlled parameters of the semi-active tuned wedge damper are highlighted in gray. Thus, the wedge angle α of the outer segments and the prestress displacement $\Delta\ell$ are subjected to controlled variations. The implementation of these input parameters has different levels of difficulty. The change in $\Delta\ell$ is equivalent to a change in the corresponding force generated by the third spring. Therefore, the practical realization of this parameter can be implemented by electromagnetic or piezo-actuators that generate the equivalent force. The

change of the wedge angle requires additional design and more effort; however, the changes in the flanks can be implemented with gear or cable drives.

Due to dry friction, the motion of system in Fig. 1 has two discrete phases: the stick phase and the slip phase. For a detailed derivation of the equations of motion, the reader is referred to [15], and these are given by

$$\begin{aligned} &\text{stick phase}: (m_1+m_2)\ddot{x}_1 + c_1 x_1 = F\sin\Omega t\,, \\ &\qquad\qquad \dot{x}_2 = \dot{x}_1\,, \end{aligned} \tag{1}$$

$$\begin{aligned} &\text{slip phase}: m_1\ddot{x}_1 + c_1 x_1 - F_{\mathrm{TWD}} = F\sin\Omega t\,, \\ &\qquad\qquad m_2\ddot{x}_2 + F_{\mathrm{TWD}} = 0\,, \\ &\qquad\qquad F_{\mathrm{TWD}} = c_2(x_2-x_1) + 2c_3\,(2y+\Delta\ell)\,\frac{y_x+\mu\,\mathrm{sgn}(\dot{x}_2-\dot{x}_1)}{1-\mu y_x\,\mathrm{sgn}(\dot{x}_2-\dot{x}_1)}\,. \end{aligned} \tag{2}$$

In Eq. (2), μ represents the friction coefficient between the secondary mass and the contact surfaces. Additionally, y and y_x describe the contact surface geometry. The function y describes the vertical displacement of the contact surfaces dependent on the relative displacement $x_{\mathrm{rel}} = x_2 - x_1$, whereas y_x describes the tangent of the momentary contact angle. These functions are visualized in Fig. 2 and given by

$$y = \begin{cases} -\tan\alpha(x_{\mathrm{rel}}+\Delta_2) + r(1-\cos\alpha), & x_{\mathrm{rel}} < -\Delta_2 \\ r - \sqrt{r^2-(x_{\mathrm{rel}}+\Delta_1)^2}, & -\Delta_2 < x_{\mathrm{rel}} < -\Delta_1 \\ 0, & |x_{\mathrm{rel}}| < \Delta_1 \\ r - \sqrt{r^2-(x_{\mathrm{rel}}-\Delta_1)^2}, & \Delta_1 < x_{\mathrm{rel}} < \Delta_2 \\ \tan\alpha(x_{\mathrm{rel}}-\Delta_2) + r(1-\cos\alpha), & \Delta_2 < x_{\mathrm{rel}} \end{cases}, \tag{3}$$

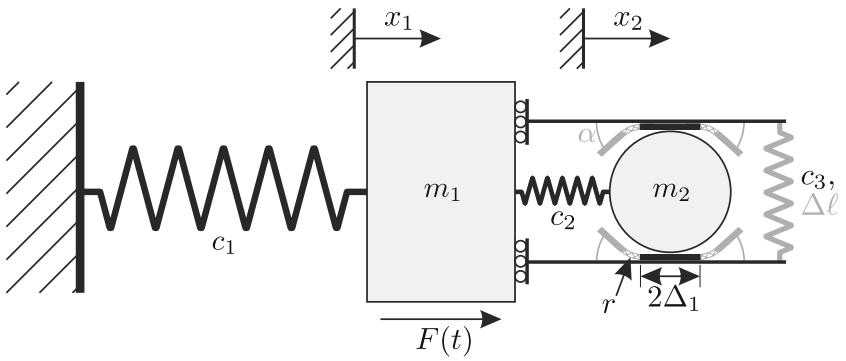

Fig. 1 Schematic model of the semi-active tuned wedge damper

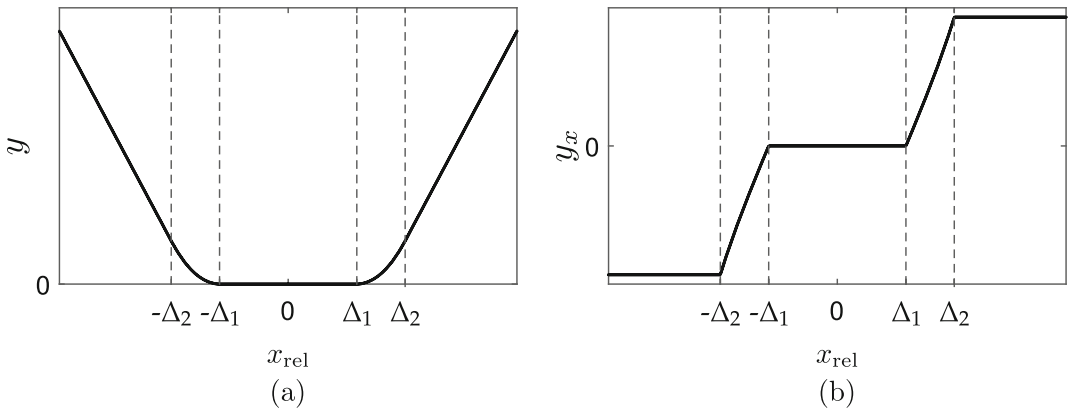

Fig. 2 **a** Contact function geometry y and **b** derivative of the contact function geometry y_x with respect to the relative displacement x_{rel}

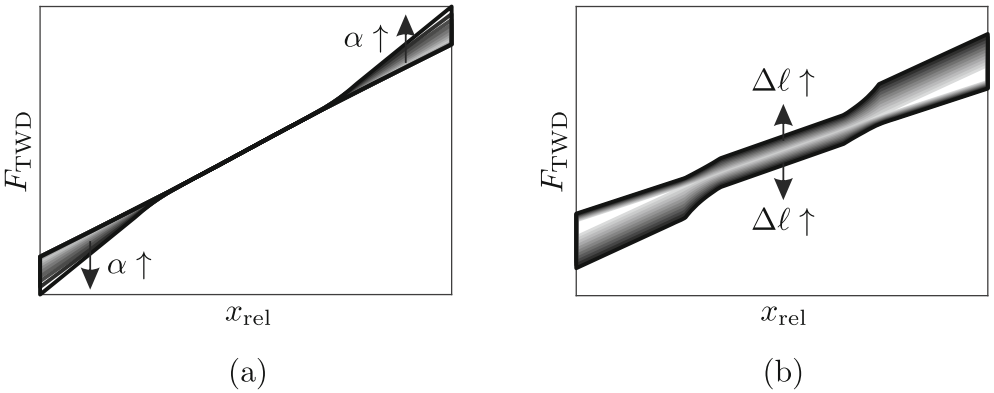

Fig. 3 Schematic representation of the effects of the input parameters on the tuned wedge damper force: **a** wedge angle α variation for $\Delta\ell = 0$ m and **b** prestress displacement $\Delta\ell$ variation

$$y_x = \frac{\mathrm{d}y(x_{\mathrm{rel}})}{\mathrm{d}x_{\mathrm{rel}}}\,. \tag{4}$$

The transition from sliding to sticking is determined by the sticking conditions. Accordingly, the transition into sliding is determined by the failure to comply with these conditions. The sticking conditions are described by

$$F_{c_3} = c_3(2y + \Delta\ell)\,, \tag{5}$$

$$H = \frac{m_2}{m_1 + m_2}(F\sin\Omega t - c_1 x_1) + c_2(x_2 - x_1)\,, \tag{6}$$

$$R = -\frac{2F_{c_3}y_x + H}{2\sqrt{1+y_x^2}} \quad \text{and} \quad R_{\max} = \mu N = \mu\frac{2F_{c_3} - Hy_x}{2\sqrt{1+y_x^2}}\,, \tag{7}$$

$$|R| < R_{\max}\,, \quad \text{and} \quad \dot{x}_1 = \dot{x}_2\,. \tag{8}$$

To obtain a deeper insight into the damper's dynamics, the damper force is decomposed into two parts: a dissipation-free stiffness force $F_{\mathrm{TWD,c}}$ and a dissipative force $F_{\mathrm{TWD,d}}$. These forces are given by

$$F_{\mathrm{TWD}} = F_{\mathrm{TWD,c}} + F_{\mathrm{TWD,d}}\,, \tag{9}$$

$$F_{\mathrm{TWD,c}} = F_{\mathrm{TWD}}(\mu = 0) = c_2(x_2 - x_1) + 2c_3(2y + \Delta\ell)y_x\,, \tag{10}$$

$$F_{\mathrm{TWD,d}} = F_{\mathrm{TWD}} - F_{\mathrm{TWD,c}} = \frac{2\mu c_3(2y + \Delta\ell)(1+y_x^2)}{1 - \mu y_x \mathrm{sign}(\dot{x}_2 - \dot{x}_1)}\mathrm{sign}(\dot{x}_2 - \dot{x}_1)\,. \tag{11}$$

As is noted from Eq. (11), the dissipative force depends on the relative displacement. Integrating $F_{\mathrm{TWD,d}}$ over the distance yields the dissipated mechanical energy W_{d}. For harmonic oscillations with a relative amplitude lower than Δ_1, W_{d} is proportional to the relative vibration amplitude, i.e., $W_{\mathrm{d}} \sim A_{\mathrm{rel}}$. For harmonic oscillations and oscillation with a relative amplitude larger than Δ_1, W_{d} is proportional to the squared value of the relative vibration amplitude, i.e., $W_{\mathrm{d}} \sim A_{\mathrm{rel}}^2$. For more details regarding the exact expressions of W_{d}, the reader is referred to [15].

The qualitative influence of the input parameters α and $\Delta\ell$ on the damper force F_{TWD} is presented in Fig. 3. Changes in the prestress displacement are equivalent to modulations of the normal force pressing the contact surfaces onto the secondary mass. An increase in both of these parameters leads to higher dissipation. The difference lies in the way the dissipation is introduced. Higher values of the angle α lead to increasing dissipation only in the outer segments, whereas higher prestress values increase the dissipation over the whole oscillation range. From a geometrical point of view, the wedge angle changes the opening angle of the outer force hysteresis, and the prestress displacement changes the width of the whole force hysteresis. Furthermore, their influence on the dissipated energy is also different. The higher angles increase the dissipated energy proportional to the square of the relative amplitude A_{rel}^2. In contrast, the prestress increment affects only the dissipated energy proportional to the relative amplitude A_{rel}, c.f. Eq. (11). The control strategies vary both of these parameters to introduce dissipation in a targeted manner with low friction coefficients.

The following sections compare the two control strategies to their passive counterpart. Three excitation cases are considered: a rectangular pulse excitation, a sweep excitation, and an application scenario. The rectangular pulse gives insight into the transient behavior of the strategies, whereas the sweep excitation gives an approximation for the stationary behavior. The application scenario provides information about the suitability of the control strategies for more realistic applications. The sum of insights obtained via the excitation simulations yields the theoretical basis for a semi-active implementation of the tuned wedge damper.

In the first case, the system is let go from nontrivial initial conditions, and the free behavior is investigated. Afterward, a force in the form of a rectangular pulse is applied. This excitation yields insights into the transient behavior of the control strategies. Understanding into the strategies' reaction to harsh excitation is also obtained. The excitation force in this case is given by

$$F_{\mathrm{rect}}(t) = \begin{cases} 0, & t_0 \leq t < t_1 \\ F_0, & t_1 \leq t < t_2 \\ 0, & t_2 \leq t < t_3 \end{cases}$$

with

$$F_0 = 0.01\,\mathrm{N},\ t_0 = 0\,\mathrm{s},\ t_1 = 200\,\mathrm{s},\ t_2 = 300\,\mathrm{s},\ t_3 = 325\,\mathrm{s}\,.$$

In the second case, a sweep excitation is applied and the analysis is focused on the system's almost stationary behavior. The system starts with zero initial conditions, and a frequency range including both structural resonances and the absorption frequency is slowly passed through. This yields an approximation of the controlled systems' response at different excitation frequencies. The sweep excitation is described by

$$F_{\mathrm{sweep}}(t) = F_0 \sin(\varphi_{\mathrm{sweep}}(t))$$

with

$$\varphi_{\mathrm{sweep}}(t) = \int_0^t \Omega_{\mathrm{sweep}}(\tau)\mathrm{d}\tau\ ,\ \Omega_{\mathrm{sweep}}(t) = \frac{\Omega_1 - \Omega_0}{t_1 - t_0}(t - t_0) + \Omega_0\,,$$
$$F_0 = 0.01\,\mathrm{N},\ t_0 = 0\,\mathrm{s}\,,\ t_1 = 10^5\,\mathrm{s}\,,\ \Omega_0 = 0\,\mathrm{rad/s},\ \Omega_1 = 2\,\mathrm{rad/s}\,.$$

The third case considers an application scenario. First, a run-up to the system's operation frequency is performed starting from zero initial conditions. This is followed by a nominal operation range with a harmonic excitation. Subsequently, an overload section is simulated, in which the excitation amplitude rises tenfold. Afterward, the excitation is brought again to its original level in the recovery phase. Finally, the system is shut down in a controlled manner. In this phase, the excitation force and the excitation frequency linearly approach zero. The consideration of both the system run-up and run-down has the advantage that nonlinear phenomena in the system response are taken into account. The scenario force is given by

$$F_{\mathrm{scen}}(t) = F_{\mathrm{A,scen}}(t) \sin(\varphi_{\mathrm{scen}}(t))\,.$$

The key components of $F_{\mathrm{scen}}(t)$ are visualized in Fig. 4 and given by

$$F_{\mathrm{A,scen}}(t) = \begin{cases} F_0, & t_0 \leq t < t_2 \\ \dfrac{F_3 - F_2}{t_3 - t_2}(t - t_3) + F_3, & t_2 \leq t < t_3 \\ \dfrac{F_4 - F_3}{t_4 - t_3}(t - t_4) + F_4, & t_3 \leq t < t_4 \\ \dfrac{F_5 - F_4}{t_5 - t_4}(t - t_5) + F_5, & t_4 \leq t < t_5 \end{cases},$$

$$\varphi_{\mathrm{scen}}(t) = \int_0^t \Omega_{\mathrm{scen}}(\tau)\mathrm{d}\tau\ ,\ \Omega_{\mathrm{scen}}(t) = \begin{cases} \dfrac{\Omega_1 - \Omega_0}{t_1 - t_0}(t - t_0) + \Omega_0, & t_0 \leq t < t_1 \\ \Omega_1, & t_1 \leq t < t_4 \\ \dfrac{\Omega_5 - \Omega_4}{t_5 - t_4}(t - t_5) + \Omega_5, & t_4 \leq t < t_5 \end{cases},$$

$$F_0 = F_1 = F_2 = 0.01\,\mathrm{N},\ ,\ F_3 = 10F_0,\ F_4 = F_0,\ F_5 = 0\,\mathrm{N},$$

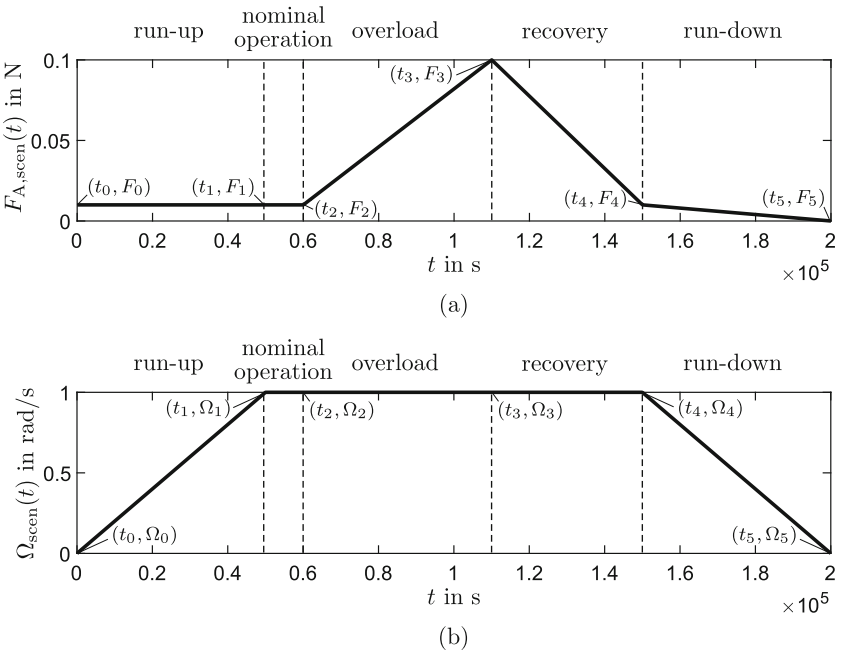

Fig. 4 Components of the scenario excitation: **a** force amplitude $F_A(t)$ and **b** angular frequency $\Omega(t)$

$$\Omega_0 = 0\,\text{rad/s},\ \Omega_1 = \Omega_2 = \Omega_3 = \Omega_4 = 1\,\text{rad/s},\ \Omega_5 = 0\,\text{rad/s},$$
$$t_0 = 0\,\text{s},\ t_1 = 5{\cdot}10^4\,\text{s},\ t_2 = 6{\cdot}10^4\,\text{s},\ t_3 = 11{\cdot}10^4\,\text{s},\ t_4 = 15{\cdot}10^4\,\text{s},\ t_4 = 20{\cdot}10^4\,\text{s}\,.$$

The initial conditions are given with the state vector $\mathbf{x}_0 = [x_{10}, x_{20}, \dot{x}_{10}, \dot{x}_{20}]^\top$. The initial conditions are chosen $\mathbf{x}_{0,\text{rect}} = [1, 1, 1, 1]^\top$ and $\mathbf{x}_{0,\text{sweep}} = \mathbf{x}_{0,\text{scen}} = [0, 0, 0, 0]^\top$ depending on the excitation. Furthermore, the constant parameters of the tuned wedge damper are

$$m_1 = 1\,\text{kg},\ m_2 = 0.1\,\text{kg},\ c_1 = 1\,\text{N/m},\ c_2 = 0.1\,\text{N/m},\ c_3 = 0.01\,\text{N/m},$$
$$\Delta_1 = 0.1\,\text{m},\ r = 0.01\,\text{m},\ \mu = 0.1\,.$$

Note that all these values (masses, lengths, forces and time intervals) have to be considered as relative values and should not lead to misinterpretations. All the results should be scaled to realistic application conditions. The angle and prestress displacement for the passive system are given by $\alpha_{\text{pa}} = 20°$ and $\Delta\ell_{\text{pa}} = 0\,\text{m}$. The input parameters of the semi-active system are limited to $\alpha \in [0, \alpha_{\max}]$ and $\Delta\ell \in [0, \Delta\ell_{\max}]$. The limits $\alpha_{\max}$ and $\Delta\ell_{\max}$ are specified for each control strategy later on and provide more realistic working conditions for the semi-active systems.

3 Skyhook Control

The Skyhook Control emulates, when possible, a damper attached to an inertial frame, regardless of the actual damper position [9]. Furthermore, this is a dissipation-oriented control strategy. Since in this case the strategy is implemented for vibration damping instead of vibration isolation, it is similar to Dupont's Lyapunov-based controller. The basic strategy is taken from Dupont [8]; however, modifications such as a regularization, to ensure smooth transitions, and clipping, to avoid sticking, are taken into account. To implement the Skyhook Control, it is first verified if the structure of dissipative forces is in accordance with the control strategy. Subsequently, the algorithm for the inputs is defined. Additionally, the input force is clipped to avoid sticking. Lastly, the section concludes with the simulations of the Skyhook Control behavior and its comparison to the passive system.

The Skyhook Control assumes dissipative forces of the form $F_{\text{Sky}} = |F_{\text{TWD,d}}|\text{sign}(\dot{x}_2 - \dot{x}_1)$, where the direction of the force is solely defined by the relative velocity. From Eq. (11), the dissipative force does not strictly comply with this form. This is due to the denominator, which can change signs depending on the relative velocity. However, for all practical purposes, this is not the case. Since the maximum input angle is limited

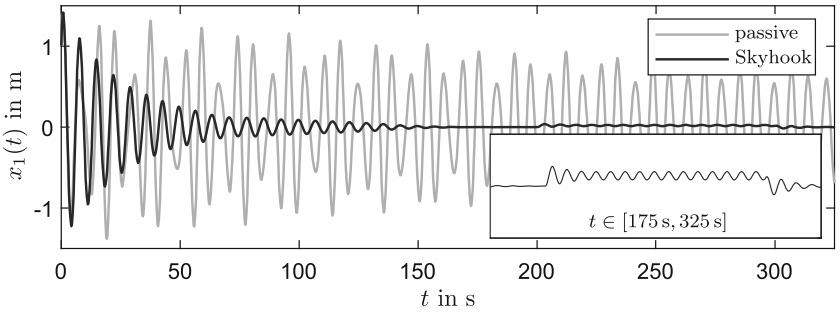

Fig. 5 Response of the Skyhook Control to the rectangular pulse

to $\alpha_{\max} \leq 45°$, y_x has a maximum value of 1. Furthermore, since low friction coefficients are investigated ($\mu < 1$), it is not possible for the denominator to change signs. Taking into account the input limitations, the force in Eq. (11) complies with the necessary structure for the implementation of the control strategy.

The Skyhook Control defines a damper force that generates a braking effect on the main mass. This is only possible when the relative velocity between the masses and the absolute velocity of the main mass have different signs, i.e., $\dot{x}_1(\dot{x}_2 - \dot{x}_1) < 0$. When this is not the case, the damper force accelerates the main mass. To avoid exacerbating the oscillation of the main mass, the damper force is set to zero in these cases, i.e., when $\dot{x}_1(\dot{x}_2 - \dot{x}_1) > 0$. This results in the control structure from Dupont [8], i.e.,

$$F_{\mathrm{TWD,d}} = \begin{cases} F_{\mathrm{TWD,d,max}}, & \dot{x}_1(\dot{x}_2 - \dot{x}_1) < 0 \\ 0, & \dot{x}_1(\dot{x}_2 - \dot{x}_1) > 0 \end{cases} . \tag{12}$$

The input parameters are calculated to ensure Eq. (12) and maximize the braking effect. For the wedge angle, this leads to a maximization of the input angle. The prestress displacement is maximized under the condition that sticking is avoided. If sticking occurs, no relative movement is observed, and therefore, no energy is dissipated. Since this strategy is solely based on damping, sticking is counterproductive. The prestress displacement is thus calculated to comply with the slipping condition $|R| = \mu N > R_{\max}$, c.f. Eqs. (7) and (8). Additionally to ensure smooth transitions between the extreme values, a regularization is applied with the hyperbolic tangent function and the regularization parameter $\varepsilon_{\mathrm{Sky}}$. This leads to

$$\alpha_{\mathrm{Sky}} = \frac{\alpha_{\max}}{2}\left(1 - \tanh\left(\frac{(\dot{x}_2 - \dot{x}_1)\dot{x}_1}{\varepsilon_{\mathrm{Sky}}}\right)\right), \tag{13}$$

$$\Delta\ell_{\mathrm{Sky}} = \frac{\Delta\ell_{\max}(R, R_{\max})}{2}\left(1 - \tanh\left(\frac{(\dot{x}_2 - \dot{x}_1)\dot{x}_1}{\varepsilon_{\mathrm{Sky}}}\right)\right). \tag{14}$$

Once the desired input parameters are known, the actual input parameters are changed accordingly. However, this change is not instantaneous; instead, the input variation is modeled dynamically with two first-order systems

$$\dot{\alpha} = -\lambda_{\mathrm{Sky}}(\alpha - \alpha_{\mathrm{Sky}}) \quad \text{and} \quad \dot{\Delta\ell} = -\lambda_{\mathrm{Sky}}(\Delta\ell - \Delta\ell_{\mathrm{Sky}}) \tag{15}$$

where λ_{Sky} is a measure of how fast the input parameters are changed. This input modeling approach has the advantage that it takes into account oscillations introduced by the change of the input parameters.

The parameters of the Skyhook Control Strategy are determined by trial and error and given by

$$\alpha_{\max,\mathrm{Sky}} = 20°,\ \Delta\ell_{\max,\mathrm{Sky}} = 240\,\mathrm{m},\ \lambda_{\mathrm{Sky}} = 0.64\,\mathrm{s}^{-1},\ \varepsilon_{\mathrm{Sky}} = 0.01\,\mathrm{m}^2/\mathrm{s}^2\,.$$

Figure 5 compares the response to the impulse excitation of the Skyhook Control against its passive counterpart. The passive system introduces low dissipation which leads to a slow decay of the oscillations. In contrast, the Skyhook Control is able to introduce damping despite the low relative differences in the initial conditions. The control strategy dampens the free oscillations in the first 150 s. Furthermore, the rectangle impulse is countered effectively. The effect of the impulse on the main coordinate is minimal since in the pulse range it has a maximal value of 0.038 m. Once the excitation subsides, the amplitudes return to the vicinity of zero. At the end of the simulation, the amplitudes of the Skyhook Control are zero, whereas the amplitudes of the passive system are roughly 0.500 m.

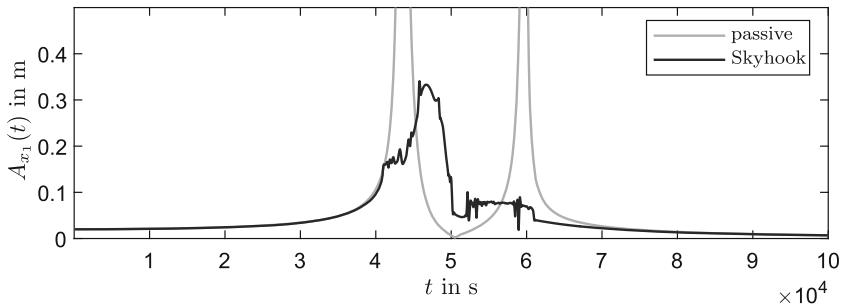

Fig. 6 Response of the Skyhook Control to the sweep excitation. Note: the maximum amplitude of the passive system is equal to 2.060 m

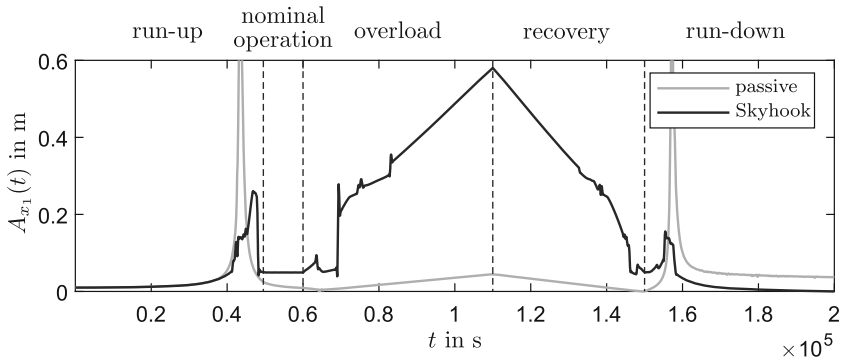

Fig. 7 Response of the Skyhook Control to the application scenario

The sweep response of the Skyhook Control is observed in Fig. 6. The amplitudes of both systems are approximately equal for frequencies outside the resonance and absorption regimes. The maximum amplitudes of the semi-active damper are substantially lower than its passive counterpart. Compared to the maximum value of 2.060 m of the passive damper, the semi-active damper has a maximum amplitude of 0.341 m, which yields a reduction of 83.57%. In the vicinity of the absorption frequency, the disadvantages of the Skyhook Control are noted. Since this strategy is dissipation-focused, the amplitudes are higher than its passive counterpart. At the absorption, the semi-active damper amplitude has a value of 0.046 m. After this regime, the amplitudes of the semi-active damper rise again and, however, remain under 0.101 m. The rise is due to the resonance regime of the second eigenfrequency.

The response to the application scenario is presented in Fig. 7. During the run-up phase, the semi-active system shows a lower maximum amplitude than its passive counterpart. The disadvantages of the semi-active system show starting from the nominal operation phase. Due to the focus on damping, the oscillation amplitudes are not minimal during this phase. Instead, they have a value of 0.049 m. Additionally, the Skyhook Control shows different amplitude ranges during the overload phase. These are caused by the changes in the maximum input values that the control allows. Due to the increased amplitude of the excitation, the maximum stiction force increases and with it the maximum value of the prestress displacement. The added possibility to introduce more dissipation leads to the different ranges in the response and the transition between them. In the overload phase, a maximum amplitude of 0.580 m is observed, which is by a factor 12.95 higher than the passive system. The passive system takes advantage of absorption and therefore has lower amplitudes. Nevertheless, the Skyhook Control still has an advantage when comparing the maximum amplitudes throughout the whole simulation, since the maximum amplitudes of the passive system are 1.0642 m. This results in an overall maximum amplitude reduction of 45.48% relative to the passive system. During the recovery phase, the amplitudes subside to the nominal operation levels. During the run-down, the system passes once again through the resonance regime, where the amplitudes rise and have a value of 0.156 m. Compared to the passive system during run-down this represents a 82.65% amplitude reduction.

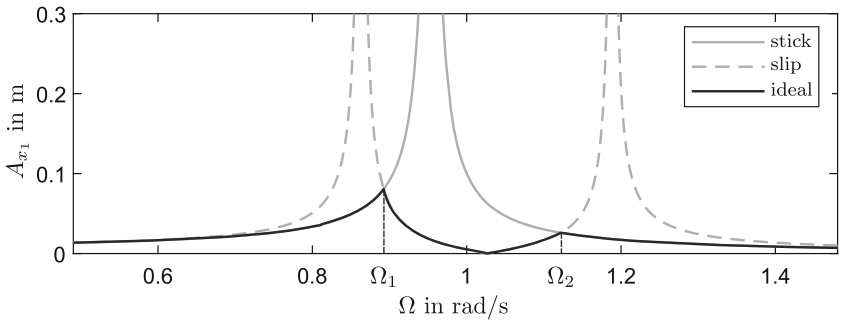

Fig. 8 Ideal change between the sticking and slipping frequency response functions

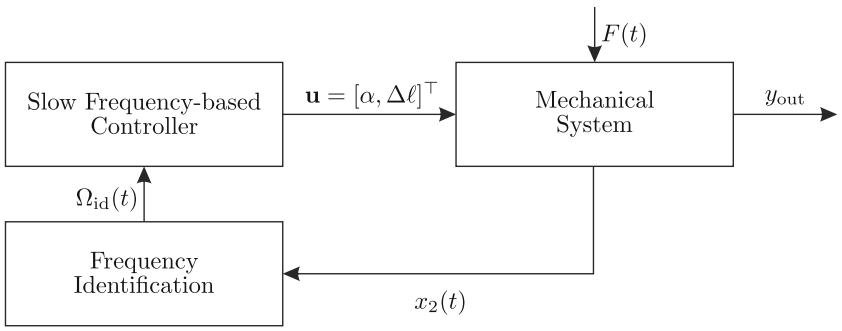

Fig. 9 Control structure of the slow frequency-based control

4 Slow frequency-based control

The slow frequency-based control (SFC) uses prior knowledge of the systems and defines the system parameters accordingly. In this case, the prior knowledge used is based on the frequency response of the passive tuned wedge damper. To describe the slow frequency-based control, first, the ideal change of the control strategy is described. Second, the control structure, as well as the necessary frequency identification, is presented. Third, the rule for the parameter choice is formulated. Lastly, the simulations of the semi-active control strategy are presented.

This control method uses knowledge of the frequency response to determine the system parameters. The two frequency responses and an ideal case, are plotted in Fig. 8. The figure shows the responses of the sticking ($\Delta\ell \to \infty$) and slipping ($\Delta\ell = 0$) systems. The sticking response is modeled with Eq. (1), and the slipping response corresponds to an undamped tuned mass damper with the secondary stiffness $c_{\text{eff,res}} = c_2 + 4c_3 \tan^2 \alpha$. The ideal response is built by selecting the branch with the lowest amplitude. The ideal response has the advantages of low vibration amplitudes without having to forgo an absorption frequency. The slow frequency-based control method aims to reproduce this ideal curve. The underlying basic principle of the system is the change in the system's structure caused by the transitions between sticking and slipping. As the system transitions, the eigenfrequencies change from two slipping eigenfrequencies to a single sticking frequency or vice versa. The targeted change aims to avoid structural resonances and achieve absorption.

The overall control structure is shown in Fig. 9 and consists of three blocks: the mechanical system, the frequency identification, and the controller. To influence the mechanical system, the two input parameters α and $\Delta\ell$ are varied. These two parameters serve as inputs to the mechanical system. This block contains and simulates the equations of motion of the tuned wedge damper with the corresponding parameters. The resulting movement of the auxiliary mass $x_2(t)$ is recorded and passed to the frequency identification block. This variable is chosen since it does not tend to zero in the absorption regime. This simplifies the identification. The identification block detects the main frequency of the system using a Fourier Transformation. The identified frequency Ω_{id} is then passed on to the controller, which sets the parameters α and $\Delta\ell$. The idea of this controller is based on the adaptive gain scheduling [16]. It is similar in the sense that an additional quantity, the identified frequency, is used, to gain additional knowledge of the system. However, it is noted that the structure in Fig. 9 is that of the open-loop control, since the output is not fed back to the system. Furthermore, as is stated later on, the strategy does not change the parameters of a controller, but instead directly defines the desired input parameters.

The controller determines the desired input values α_{SFC} and $\Delta\ell_{\mathrm{SFC}}$ according to

$$\alpha_{\mathrm{SFC}} = \begin{cases} \alpha_{\mathrm{max,SFC}}, & \Omega_1 \le \Omega_{\mathrm{id}} \le \Omega_2 \\ 0, & \text{else} \end{cases}, \tag{16}$$

$$\Delta\ell_{\mathrm{SFC}} = \begin{cases} 0, & \Omega_1 \le \Omega_{\mathrm{id}} \le \Omega_2 \\ \Delta\ell_{\mathrm{max,SFC}}, & \text{else} \end{cases}. \tag{17}$$

In Eqs. (16) and (17), Ω_1 and Ω_2 represent the crossing frequencies between the linear sticking and slipping systems. Outside the Ω_1-Ω_2-range, the lowest amplitudes are achieved by the sticking system. Thus, the system parameters are chosen so that the tuned wedge damper sticks. The outer segments are flat and the prestress displacement is maximized. In the Ω_1-Ω_2-range, absorption is the chosen vibration reduction mechanism. To this end, the prestress is set to zero to minimize damping horizontal section, i.e., in the $2\Delta_1$-range. Additionally, the wedge angle α is maximized to insert damping strictly outside the $2\Delta_1$-range. This parameter choice funnels large oscillations into the dissipation-free range. The control strategy highly depends on the identified frequency since the parameters are solely determined by it. This is problematic in the presence of noise in the measured signal. This is manageable by applying a low pass filter to the measured signal provided the magnitude of the noise is small compared to $x_2(t)$. The frequencies Ω_1 and Ω_2 are calculated based on the crossings of the linear stick and slip systems in Fig. 8. First the frequency response functions are equated, and afterward, the equations are solved for the frequency where the crossings occur. These are independent of the excitation amplitude and are given by

$$\Omega_{1,2} = \omega_{01}\sqrt{\frac{\gamma + (1+\gamma)p^2 \mp \sqrt{(1+\gamma)^2 p^4 - 2\gamma p^2 + \gamma^2}}{\gamma(2+\gamma)}} \tag{18}$$

$$\text{with } \gamma = \frac{m_2}{m_1},\ p^2 = \frac{c_{2,\mathrm{eff}}}{c_1},\ \omega_{01}^2 = \frac{c_1}{m_1},\ c_{2,\mathrm{eff}} = c_2 + 4c_3 \tan^2 \alpha_{\mathrm{max,SFC}}\,.$$

As with the aforementioned strategy a dynamic input model is considered, with the rate of change for the inputs λ_{SFC}, the differential equations for the inputs are given by

$$\dot{\alpha} = -\lambda_{\mathrm{SFC}}(\alpha - \alpha_{\mathrm{SFC}}) \quad \text{and} \quad \dot{\Delta\ell} = -\lambda_{\mathrm{SFC}}(\Delta\ell - \Delta\ell_{\mathrm{SFC}})\,. \tag{19}$$

The slow frequency-based control does not aim to counter vibration in the lapse of one oscillation. Instead, it focuses on the attenuation of vibrations over a large time frame. It is therefore important that the changes of the parameter do not introduce high frequency oscillations in the system since the control strategy cannot promptly react to these. To this end, the rate of change λ_{SFC}, the maximum wedge angle $\alpha_{\mathrm{max,SFC}}$, and the maximum prestress displacement $\Delta\ell_{\mathrm{max,SFC}}$ are chosen as small. However, not unreasonably small such that vibration reduction is not realized. The first two parameters are found by trial and error. The maximum prestress value is approximated with the amplitude at the transition $A_L(\Omega_1)$ [15]. From the parameters of the passive system and the amplitude of the excitation, the maximum value results in

$$\Delta\ell_{\mathrm{max,SFC}} = \frac{A_L(\Omega_1)\Omega_1^2 m_2}{2c_3\mu} \quad \text{with} \quad A_{\mathrm{L}}(\Omega_1) = \frac{F_0}{|c_1 - (m_1+m_2)\,\Omega_1^2|}\,. \tag{20}$$

Although the parameter F_0 is found in Eq. (20), the exact value is not required. Equation (20) is meant as an estimate for the maximum prestress value, accordingly an estimate of the magnitude order of F_0 is sufficient. The expression above yields the minimal prestress displacement to ensure that the system sticks until Ω_1.

The parameters for the slow frequency-based control are chosen as

$$\alpha_{\mathrm{max,SFC}} = 20^\circ,\ \Delta\ell_{\mathrm{max,SFC}} = 3.219\,\mathrm{m},\ \lambda_{\mathrm{SFC}} = 0.001\,\mathrm{s}^{-1},\ F_0 = 0.01\,\mathrm{N},$$
$$N = 256,\ t_{\mathrm{s}} = 1\,\mathrm{s},\ \Omega_1 = 0.892\,\mathrm{rad/s},\ \Omega_2 = 1.122\,\mathrm{rad/s}\,.$$

The behavior in response to the rectangular impulse is presented in Fig. 10. Although the control strategy is not designed for the transient response, it effectively reduces the oscillation amplitudes. The amplitudes nearly vanish in the first 200 s of the simulation. During the rectangular pulse, the amplitudes rise to 0.080 m. At the end of the simulation, an amplitude reduction of 91.83% is achieved. However, small oscillations remain in the semi-active system and have an amplitude of 0.049 m.

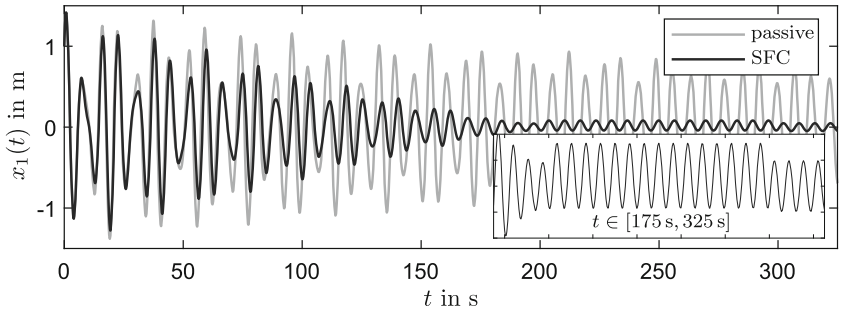

Fig. 10 Response of the slow frequency-based control to the rectangular pulse

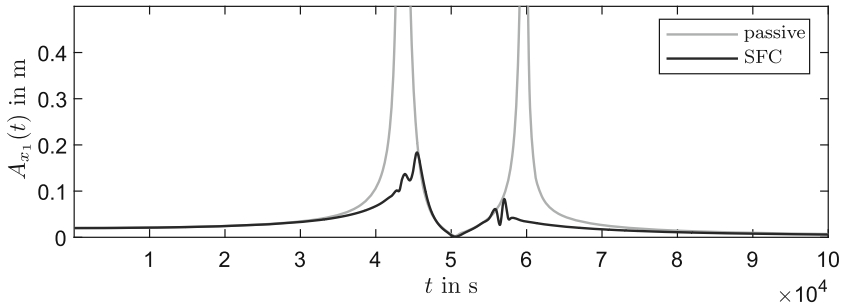

Fig. 11 Response of the slow frequency-based control to a sweep excitation

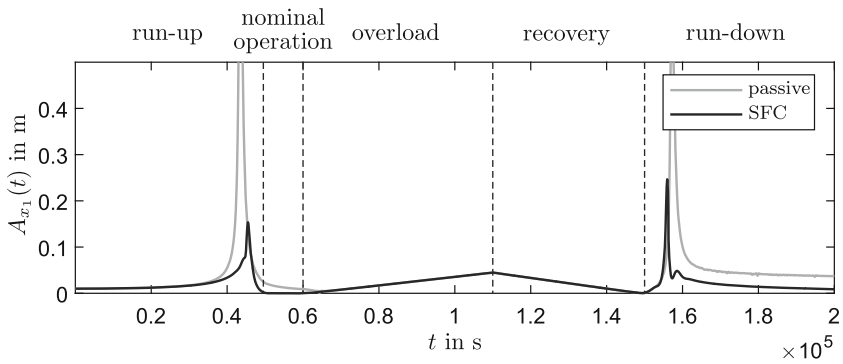

Fig. 12 Response of the slow frequency-based control to the application scenario

Figure 11 depicts the sweep response of the slow frequency-based control. Although the ideal change is not precisely realized, the control strategy has an advantageous response. It follows the sticking system on the outer frequency range and in the vicinity of the absorption it follows the passive system. Due to the changes in the wedge angle during the transition between the sticking and slipping systems, oscillations in the maximum amplitude are noted. Furthermore, a maximum amplitude of 0.180 m is noted. This results in a 91.11% amplitude reduction compared to the passive system. With the targeted stick–slip transition, the resonance frequencies are avoided and the advantages of sticking and slipping are combined.

The response of the slow frequency-based control to the application scenario is presented in Fig. 12. The strategy results in a significant improvement on the passive system. During the run-up phase, the control strategy shows a maximum amplitude of 0.154 m, which is 85.56% lower than the passive system. Since the maximum amplitude of the passive system is larger, it is not able to realize full absorption during the nominal operation range. In contrast, the amplitudes of the slow frequency-based control are in the vicinity of zero. Both systems show the same response during the overload and recovery phase and have a maximum amplitude of 0.045 m. During the run-down phase, the oscillation amplitudes rise again. The maximum amplitude in this range is higher than during the run-up phase and has a maximum value of 0.247 m. This amplitude equates to a 75.55% amplitude reduction compared to its passive counterpart.

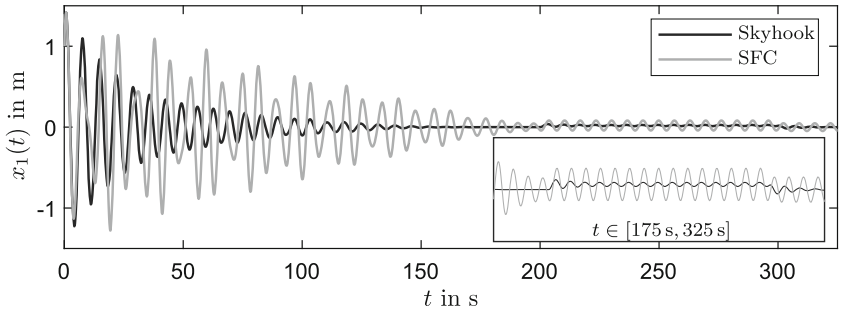

Fig. 13 Comparison of the control strategies for the rectangular pulse

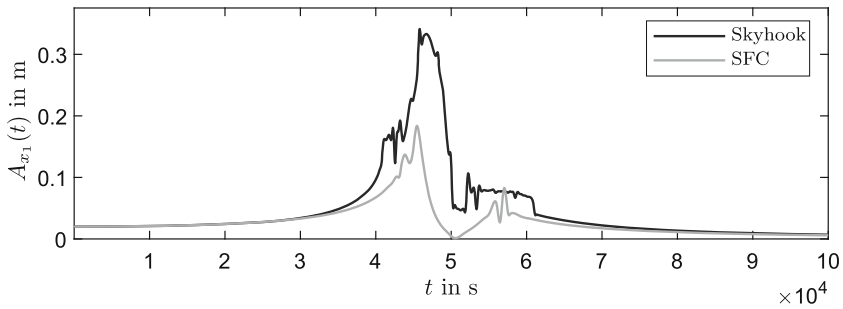

Fig. 14 Comparison of the control strategies for the sweep excitation

5 Control strategy comparison

After investigating the control strategies separately, the focus is set on their comparison. The comparison is carried out according to the aforementioned excitations. First, the rectangular pulse is considered. Second, the sweep excitation is taken into account. Finally, the strategies are compared in the application scenario.

Figure 13 portrays the comparison of the control strategies in response to the rectangular pulse. The Skyhook Control shows the best results since its approach attenuates vibrations faster. Additionally, it brings the system to a halt. The slow frequency-based control takes longer to mitigate the vibrations. Large oscillations are reduced even though this strategy was not designed for transient behavior. The amplitude of the Skyhook Control in reaction to the rectangular pulse is smaller by a factor of 2.16. In the end, the slow frequency-based control does not bring the system to a halt and small oscillations remain.

The comparison of the semi-active control strategies' response to the sweep excitation is presented in Fig. 14. The slow frequency-based control yields the best response. It has a maximal amplitude of 0.180 m which is 46.14% lower than the Skyhook Control. Furthermore, in the absorption range, the slow frequency-based control achieves the lowest amplitudes. It uses vibration absorption as its primary vibration reduction mechanism and only dissipates energy when the oscillations are partly outside the $2\Delta_1$-range. Outside the resonance and absorption regimes, the control strategies yield approximately the same results.

Figure 15 shows the comparison of the semi-active control strategies in the application scenario. The slow frequency-based control still shows the lowest amplitudes. This establishes the advantages of absorption and shifting structural resonances via sticking as effective vibration reduction mechanisms. This is noted from the run-up to the recovery phase and confirms that dissipation is not always the best vibration reduction strategy. During the overload phase, the slow frequency-based control achieves the lowest maximal amplitudes of 0.045 m. These are 92.28% smaller than the Skyhook Control. The slow frequency-based control only shows a suboptimal response during the run-down phase. During this phase, the oscillations of the slow frequency-based control are 1.58 times higher than the Skyhook Control. Considering that the slow frequency-based control shows almost overall the lowest amplitudes, its behavior represents the optimal response.

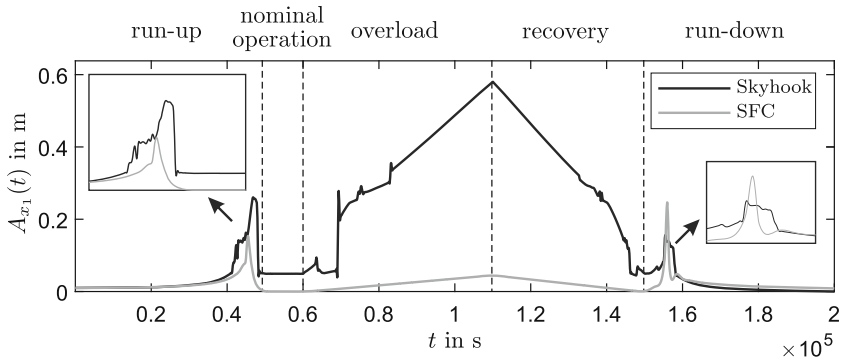

Fig. 15 Comparison of the control strategies for the application scenario

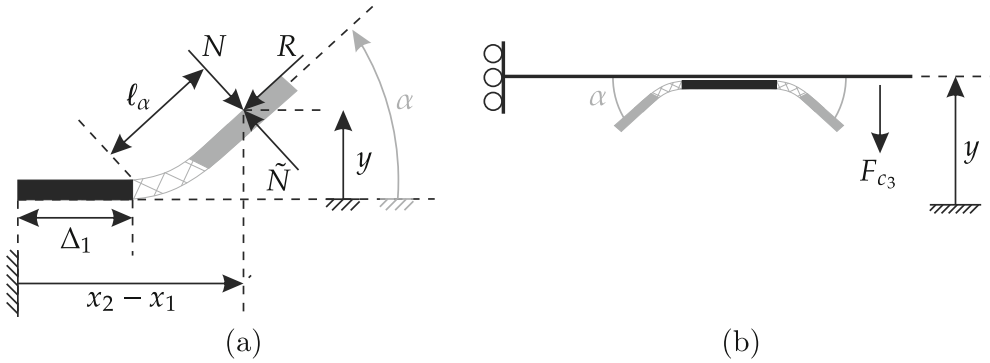

Fig. 16 Free body diagrams for the calculation of the necessary power and energy of **a** the wedge angel α and **b** the prestress displacement $\Delta\ell$

6 Energy investigations

The semi-active control strategies introduce dissipation in a more targeted manner compared to the passive system. This targeted dissipation yields lower amplitudes; however, too much dissipation results in a shorter service life. Therefore, a counterbalancing between amplitude reduction and life span is required. Since the control strategy suggested in this work does not solely rely on dissipation, it is able to reduce vibrations with a lower dissipated energy, thus achieving a longer damper service life and energy savings with low vibration amplitudes. To assess these qualities, the dissipated energy and the input energy of the control strategies are investigated. First, the formula for the dissipated energy is derived. Second, the expression for the input energy is formulated. Afterward, the formulas are used to evaluate the strategies in the three excitation scenarios.

The calculation of the dissipated energy $E_{\mathrm{TWD,d}}(t)$ is derived from the dissipated power $P_{\mathrm{TWD,d}}(t)$. The latter is calculated from the product of the dissipative force $F_{\mathrm{TWD,d}}$ and the relative velocity $\dot{x}_{\mathrm{rel}} = \dot{x}_2 - \dot{x}_1$. The dissipated energy is associated with the wear of materials. Increasing levels of dissipated energy lead to higher wear volume [17]. This is especially relevant for friction dampers since their surfaces are often rubbing against each other. In the optimal case, dampers are able to reduce vibration with low $E_{\mathrm{TWD,d}}(t)$-values. Lower values yield a longer damper life span. Considering Eq. (11) and the time-dependent values $\alpha(t)$ and $\Delta\ell(t)$, the dissipative power results in

$$P_{\mathrm{TWD,d}}(t) = -F_{\mathrm{TWD,d}}(t)(\dot{x}_2 - \dot{x}_1)\,. \tag{21}$$

The dissipated power is always negative since mechanical energy is taken from the system. From the expression above, the dissipated energy is calculated by integrating the dissipated power above over time. This results in

$$E_{\mathrm{TWD,d}}(t) = \int_0^t P_{\mathrm{TWD,d}}(\tau)\,\mathrm{d}\tau\,. \tag{22}$$

Since specific designs for the actuators are not considered, a conservative estimate for the minimal energy consumption is approximated. To calculate the approximation, the minimal mechanical power required by the wedge angle and the mechanical power required by the prestress displacement are approximated. The

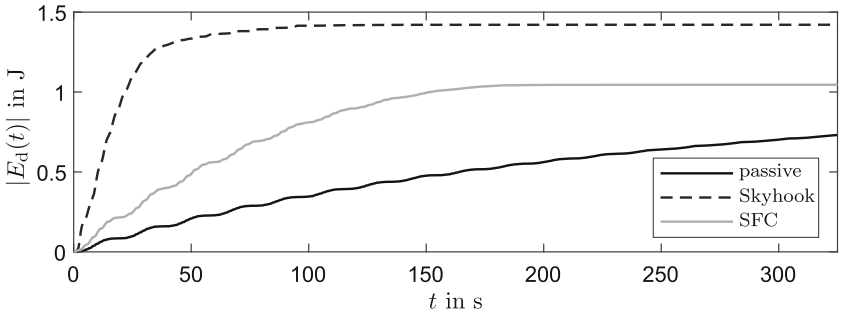

Fig. 17 Comparison of the dissipated energy for the rectangular pulse

input power of the wedge angle is estimated by considering the minimal torque M_α needed to rotate the outer flanks. This is determined by the minimal force $\tilde{N}$ to overcome the normal force N and the lever arm ℓ_α; see Fig. 16. The pivot point is assumed at the transition from the horizontal segments to the circular segments. The product of the torque $M_\alpha = \tilde{N}\ell_\alpha = N\ell_\alpha$ and the angular velocity of the outer segments $\dot{\alpha}$ yields the power associated with the angle α. Since the prestress displacement is associated with a portion of the spring force F_{c_3}, the mechanical power associated with this input is directly calculated. The input power of the prestress displacement is determined by considering the force $F_{\Delta\ell} = c_3\Delta\ell$ and the velocity with which the surfaces are pressed apart $\dot{y}$; see Fig. 16. Since the circular transition segments are small, the lever arm is approximated with

$$\ell_\alpha = \frac{1 + \operatorname{sign}(|x_2 - x_1| - \Delta_1)}{2}\sqrt{(|x_2 - x_1| - \Delta_1) + y^2}\,.$$

The dissipated power is thus given by

$$P_{\text{inputs}} = P_\alpha + P_{\Delta\ell} = 2\max(M_\alpha\dot{\alpha}, 0) + 2\max(\text{-}c_3\Delta\ell\dot{y}, 0)\,. \tag{23}$$

Analogous to the dissipated energy, the input energy results from

$$E_{\text{inputs}}(t) = \int_0^t P_{\text{inputs}}(\tau)\,\mathrm{d}\tau\,. \tag{24}$$

Equation (24) has three implicit assumptions. First, since only the mechanical power is used as the basis for the calculation, energy is only introduced with a displacement of the contact surfaces or the rotation of the outer surfaces. Energy consumption for the holding of a position is not considered. Such is the case with a self-locking design. Furthermore, an increase in the input energy due to prestress changes, while $\dot{y} = 0$, is not considered since, again, only the mechanical power is taken into account. Second, the use of the max-function considers only positive power values. Therefore, energy recovery is not considered, yielding a more conservative estimate. Third, the power associated with the angle considers only the two flanks in contact and only the minimal resistance force. The additional force required to move the flanks with a defined progression and the energy needed to move the flanks, not in contact, are not considered. Nevertheless, Eq. (24) represents a lower limit for the input energy of the control strategies. Furthermore, it allows the evaluation of the input energy of the strategies in the absence of a specific actuator model.

The equations derived above are used to evaluate the control strategies with respect to dissipated energy and input energy. First, the evaluations regarding the dissipated energy are made for the rectangular pulse, the sweep excitation, and the application scenario. Equation (22) is also applied to the passive system and compared to the semi-active control strategies. Subsequently, the evaluations for the input energy are presented for the control strategies and the aforementioned excitations.

Figure 17 shows the dissipated energy of the passive damper and the control strategies for the rectangular pulse. The Skyhook Control Strategy dissipates 1.421 J and thus dissipates the most energy. Furthermore, the dissipation is introduced in the first 106 s in a targeted manner. The slow frequency-based control dissipates less energy, namely 1.046 J. Furthermore, it requires 191 s to reach its saturation level and results in a slower strategy. The passive system does not reach a saturation level and at the end of the simulations it has the lowest dissipated energy, 0.731 J. Nevertheless, the main goal, vibration reduction, is not achieved since its vibration amplitudes are much higher than in the semi-active variants, c.f. Figs. 5 and 10. The curves show that the control strategies are able to introduce damping in a more targeted manner, which results in lower amplitudes

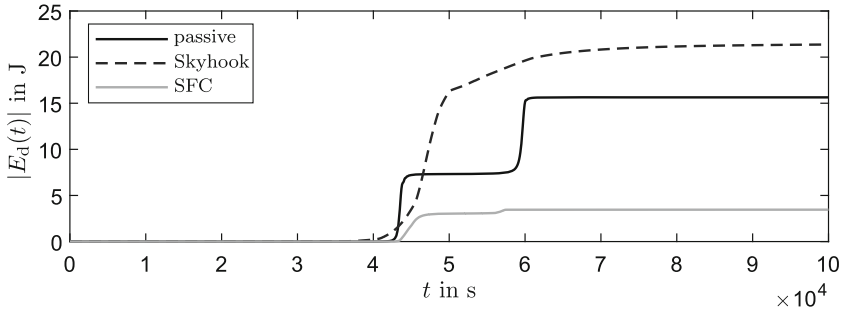

Fig. 18 Comparison of the dissipated energy for the sweep excitation

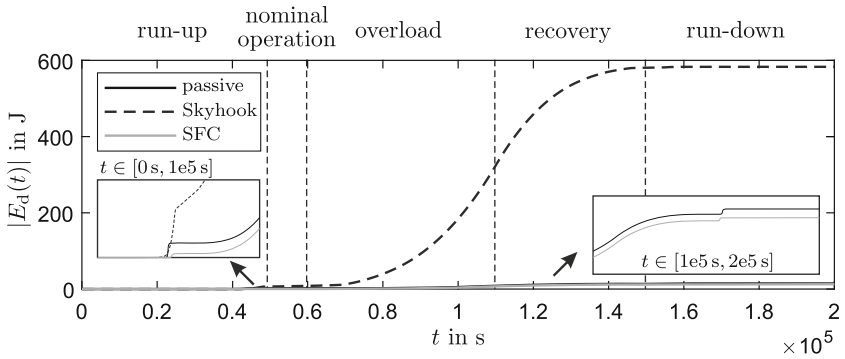

Fig. 19 Comparison of the dissipated energy for the application scenario

in a shorter time. Taking the passive system at the end of the simulation as a reference point, the dissipated energy of the slow frequency-based control and the Skyhook Control are, respectively, 43.06% and 94.42% higher than the passive system.

The dissipated energy for the sweep excitation is shown in Fig. 18. Once again the Skyhook Control shows the highest dissipated energy. Over the whole sweep range, the strategy dissipates 21.365 J. The highest increase in dissipated energy is observed between the two eigenfrequencies. However, a change is noted in the rate of change in the curve at 5e4 s. This is attributed to the phase change between the movement of the primary and secondary mass, once the absorption frequency is crossed. The passive system has the second-highest dissipation energy and two clear saturation levels, namely 7.321 J and 15.635 J. These are attributed to the passage through the two resonance frequencies. In the absorption range, the energy remains nearly constant. The control strategy with the lowest dissipated energy is the slow frequency-based control. Similar to the passive system it shows two saturation levels, but with noticeably lower energy levels. The first saturation level has a value of 3.028 J, whereas the second has a level of 3.457 J. The low dissipation is attributed to the foci of the slow frequency-based control, namely vibration absorption and structural changes via sticking. Relative to the passive system, the slow frequency-based control dissipates 77.89% less energy, whereas the Skyhook Control dissipates 36.74% more energy than its passive counterpart. This shows the advantages of combining vibration absorption and structural changes instead of solely focusing on damping.

Figure 19 shows the dissipated energy for the application scenario. The curves in the application scenario have a similar progression. The largest increases in dissipated energy are observed during the overload and recovery phases. This is mainly due to the large oscillation amplitudes. Noticeable increases are also noted at the passages through resonances during the run-up and the run-down phases. The Skyhook Control remains the strategy with the highest dissipated energy, namely 583.016 J at the end of the simulation. The passive system and the slow frequency-based control have similar results, namely 14.548 J and 12.592 J, respectively. Thus, the slow frequency-based control dissipates the least amount of energy. Compared to the passive variant, the slow frequency-based control dissipates 13.44% less energy. In contrast, the Skyhook Control dissipates 3907.45% more energy relative to the passive system.

The minimal input energy is presented in Fig. 20 for the rectangular pulse. The curves show a similar progression compared to the dissipated energy, c.f. Fig. 17. In descending order of input energy, the Skyhook Control and the slow frequency-based control consume, respectively, 1.968 J and 0.003 J. The slow frequency-

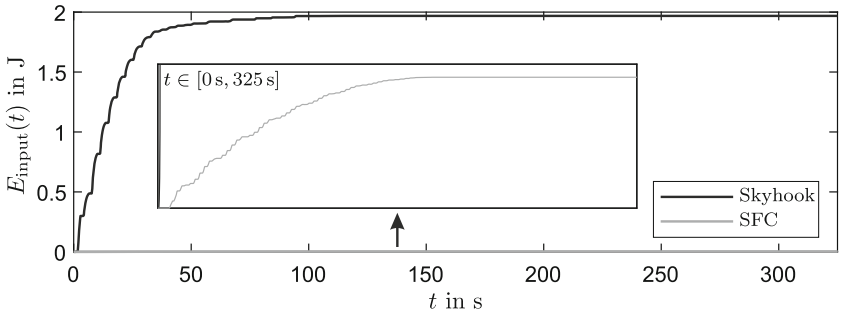

Fig. 20 Comparison of the input energy for the rectangular pulse

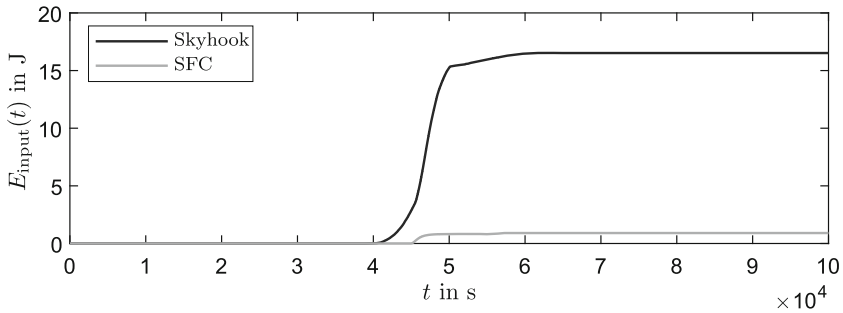

Fig. 21 Comparison of the input energy for the sweep excitation

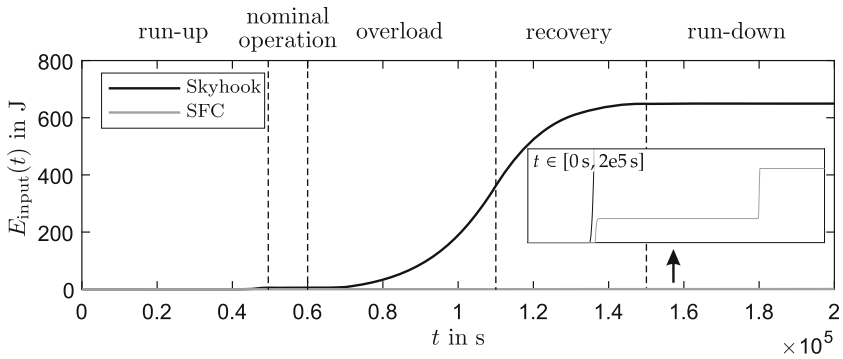

Fig. 22 Comparison of the input energy for the application scenario

based control dissipates less energy than the Skyhook Control and uses less energy to vary the wedge angle and the prestress displacement. This is due to the minimal actuation of the control strategy. Instead of reacting within a single oscillation, its long time frame leads to low input energy. It is noted that the energy used by the slow frequency control is lower than its dissipated energy. Since fully active systems directly generate the necessary force to reduce oscillations, the dissipated energy represents the minimal energy required by fully active systems. Therefore, this confirms the advantage of a semi-active system over an active system. In contrast, it shows that the Skyhook Control Strategy is not an optimal strategy for the proposed base system. Compared to slow frequency-based control, the input energy of the Skyhook Control is higher by a factor of 656.

Figure 21 shows the input energy of the control strategies for the sweep excitation. The form of the curves is the same as with the dissipated energy; however, the saturation levels are different, c.f. Fig. 18. Once again, the Skyhook Control consumes the most energy, namely 16.521 J. The slow frequency-based control has a considerably lower energy consumption with 0.907 J. A noticeable spike is noted in the input energy of the slow frequency at the passage of the first resonance frequency. The main cause for this energy spike and the strategy's higher energy consumption is the input power of the prestress displacement, which is caused by higher oscillation amplitudes of the relative coordinate during the transitions between the sticking and slipping systems. Compared to the slow frequency-based control, the input energy of the Skyhook Control is higher by a factor of 18.22.

The last observation is presented in Fig. 22 and considers the minimal input energy in the application scenario. The structure of the curves remains similar to those in Fig. 19. The Skyhook Control and the slow frequency-based control have a total input energy of 649.416 J and 0.702 J. Due to the use of absorption during the overload and recovery phase, where the oscillation amplitudes are largest, input energy of the slow frequency-based control is lower. Compared to the slow frequency-based control, the input energy of the Skyhook Control is higher by a factor of 925.803.

7 Conclusions

This section presents an assessment of the control strategies. It condenses the results of the excitation simulations and evaluates the dampers' suitability for vibration reduction. First, the Skyhook Control is addressed. Subsequently, the slow frequency-based control is evaluated. This section concludes with a short consideration of future work.

The Skyhook Control is a well-investigated control strategy, and it is taken as a reference for the developed strategy. It maximizes damping whenever possible and prevents exacerbating oscillations. The best performance of the control strategy is found in the response to the rectangular pulse. Apart from the ranges where the passive system utilizes absorption, the Skyhook Control shows an overall better response than the passive system. The disadvantages of the system are noted in the overload phase of the application scenario. The changes in the excitation amplitude lead to changes in the maximum input values. This extended input range proves counter-effective for vibration reduction. The strategy introduces more damping when absorption is the ideal damping mechanism, which leads to higher amplitudes. Energy-wise, the Skyhook Control shows the highest dissipated energy and the highest input energy. In all cases, the input energy was higher than the dissipated energy. Therefore, this strategy is not ideal for the base system since it leads to short life spans and high energy costs.

The slow frequency-based control is designed for the stationary response of the system. To this end, it measures the position of the secondary mass, identifies the oscillation frequency, and with it determines the input parameters. The parameters are chosen to realize a targeted change between sticking and slipping. It has acceptable results in transient processes. It reduces the system's vibration; however, small oscillations remain. However, these oscillations are manageable. Its sweep response is nearly optimal. The strategy avoids resonances and also achieves absorption. The advantage of the latter vibration reduction mechanism is noted in the overload phase of the application scenario. The vibrations remain smaller than the maximal amplitudes during the passage through resonance even though the excitation amplitude increases tenfold. This confirms the advantages of control strategies that are not solely dissipation-focused. It is also advantageous in slow-changing processes or in situations where the frequency characteristics of the process are known. In these cases, the frequency of the absorber is tuned to generate the best possible response. Energy-wise, this strategy provides a solution with low energy dissipation and low input energy. Therefore, the strategy results in a long service life with low energy consumption.

The proposed control strategy shows that a combination of different vibration reduction mechanisms leads to a more effective vibration mitigation. However, the quality of the strategy depends highly on the identification of the oscillation frequency. This can be problematic when more than one excitation frequency or excessive noise are involved. Furthermore, the strategy depends on the knowledge of the excitation and does not have its own adaption. A control strategy which independently adapts its vibration reduction mechanisms is still an open research topic. The design of an automated and reliable decision criterion between the vibration reduction approaches is here the main challenge. Starting points can be found in the field of adaptive multiple model control, more specifically in the works of Morse [18] and Narendra and Balakrishnan [19].

Funding Open Access funding enabled and organized by Projekt DEAL.

References

1. Wu, Q., Cole, C., Spiryagin, M., Sun, Y.Q.: A review of dynamics modelling of friction wedge suspensions. Veh. Syst. Dyn. **52**(11), 1389–1415 (2014)
2. Popp, K., Panning, L., Sextro, W.: Vibration damping by friction forces: theory and applications. J. Vib. Control **9**(3–4), 419–448 (2003)
3. Lu, Z., Wang, Z., Zhou, Y., Lu, X.: Nonlinear dissipative devices in structural vibration control: a review. J. Vib. Control **423**, 18–49 (2018)
4. Ruzicka, J.E., Derby, T.F.: Influence of Damping in Vibration Isolation vol. 7. Shock and Vibration Information Center (1971)
5. Ricciardelli, F., Vickery, B.J.: Tuned vibration absorbers with dry friction damping. Earthq. Eng. Struct. Dyn. **28**(7), 707–723 (1999)
6. Ferri, A.: Friction damping and isolation systems. J. Vib. Acoust. **117**(B), 196–206 (1995)
7. Lane, J.S., Ferri, A.A.: Optimal control of a semi-active, frictionally damped joint. In: American Control Conference, pp. 2754–2759. IEEE (1992)
8. Dupont, P., Kasturi, P., Stokes, A.: Semi-active control of friction dampers. J. Sound Vib. **202**(2), 203–218 (1997)
9. Karnopp, D., Crosby, M.J., Harwood, R.: Vibration control using semi-active force generators. J. Manuf. Sci. Eng. **96**(2), 619–626 (1974)
10. Gaul, L., Albrecht, H., Wirnitzer, J.: Semi-active friction damping of large space truss structures. Shock Vib. **11**(3–4), 173–186 (2004)
11. Lu, L.-Y.: Predictive control of seismic structures with semi-active friction dampers. Earthq. Eng. Struct. Dyn. **33**(5), 647–668 (2004)
12. Lin, G.-L., Lin, C.-C., Lu, L.-Y., Ho, Y.-B.: Experimental verification of seismic vibration control using a semi-active friction tuned mass damper. Earthq. Eng. Struct. Dyn. **41**(4), 813–830 (2012)
13. Inaudi, J.A.: Modulated homogeneous friction: a semi-active damping strategy. Earthq. Eng. Struct. Dyn. **26**(3), 361–376 (1997)
14. Laffranchi, M., Chen, L., Kashiri, N., Lee, J., Tsagarakis, N.G., Caldwell, D.G.: Development and control of a series elastic actuator equipped with a semi active friction damper for human friendly robots. Robot. Auton. Syst. **62**(12), 1827–1836 (2014)
15. Aramendiz Fuentes, J.A.: On the influence of piecewise defined contact geometries on friction dampers. PhD thesis, Karlsruher Institut für Technologie (KIT) (2022). https://doi.org/10.5445/IR/1000152268
16. Sastry, S., Bodson, M., Bartram, J.F.: Adaptive control: stability, convergence, and robustness. Acoustical Society of America (1990)
17. Stachowiak, G.W.: Wear: materials, mechanisms and practice. Wiley (2006)
18. Morse, A.S.: Supervisory control of families of linear set-point controllers-part i. Exact matching. IEEE Trans. Autom. Control **41**(10), 1413–1431 (1996)
19. Narendra, K.S., Balakrishnan, J.: Adaptive control using multiple models. IEEE Trans. Autom. Control **42**(2), 171–187 (1997)